JOURNAL OF PROPULSION AND POWER
Vol. 18, No. 5, September–October 2002

A PIV Investigation of Rotor-IGV Interactions in a Transonic Compressor

Albert J. Sanders,* John Papalia,† and Sanford Fleeter‡
Purdue University, West Lafayette, Indiana 47907

The rotor–inlet guide vane (IGV) interactions in an advanced design multistage axial compressor are experimentally investigated at both transonic and subsonic rotor operating conditions using particle image velocimetry. These benchmark blade row interaction data include measurements of the instantaneous vane-to-vane flowfield in the upstream IGV passage at 90% span for several time instants over one rotor–IGV interaction cycle. Transonic rotor–IGV interactions generate a highly unsteady IGV flowfield due to reflection and diffraction of the rotor leading-edge shocks by the IGVs. The reflected shock segments propagate upstream through the IGV passage during a rotor blade-passing period, eventually interacting with the leading-edge shock of the adjacent rotor blade before impacting the suction surface of the adjacent IGV. The high unsteady loading due to the impact of the rotor shocks with the upstream IGV row causes the vane trailing-edge stagnation point to move periodically from surface to surface over one cycle. These blade row interaction phenomena do not occur with subsonic rotor operation. The IGV unsteady backpressure variation imposed by the rotor potential field is considerably reduced, and the unsteady vane flow closely resembles the time-average vane-to-vane flow throughout the cycle.

Introduction

THE prediction of blade row interaction phenomena in transonic compressors is most challenging due to nonlinear aerodynamic and strong blade row coupling effects resulting from the highly unsteady flow. When the axial velocity component is subsonic, shocks are formed near the rotor blade leading edges that propagate into the upstream inlet guide vane (IGV) row (Fig. 1). The vane surfaces reflect and diffract these incident shocks in a complex manner, with a time-dependent wave pattern established in the vane passages due to these periodic interactions. Because turbomachine stages generally feature unequal vane–blade counts, these rotor–IGV interactions vary from passage to passage around the annulus at any time instant.

Sanders and Fleeter[1] experimentally investigated rotor–IGV interactions in an advanced design transonic multistage compressor, with the rotor-generated forcing function and resultant IGV response measured and analyzed at both design and part-speed operating conditions. The unsteady aerodynamic loading on the upstream IGVs resulting from transonic rotor–IGV interactions was very significant, with the maximum peak-to-peak static pressure fluctuations over the aft region of the vane as large as 60% of the inlet total pressure. Nonlinear interaction effects also introduced several higher harmonics into the vane response that were not present in the unsteady aerodynamic forcing function, with the pressure fluctuations on the vane aft region having components as high as $9 \times$ blade-passing frequency. These nonlinear interactions did not occur at the part-speed subsonic rotor operating condition, with both the forcing function and resultant vane response primarily first harmonic. Silkowski et al.[2] predicted these blade row interactions as part of the verification of their design codes.

Received 2 July 2001; revision received 16 March 2002; accepted for publication 18 March 2002.

*Graduate Research Assistant, School of Mechanical Engineering; currently Specialist Engineer, Honeywell Engines and Systems, Phoenix, Arizona 85284. Member AIAA.

†Graduate Research Assistant, School of Mechanical Engineering. Member AIAA.

‡McAllister Distinguished Professor, School of Mechanical Engineering. Fellow AIAA.

Eulitz et al.[3] investigated the response of an upstream stator to shocks generated by the downstream rotor in a transonic compressor using two-dimensional viscous and inviscid analyses. The inviscid analysis of three stator and two rotor passages indicated that the rotor shocks interacted strongly with the vane trailing edges, generating pressure waves that reflected off the vane surfaces multiple times as they propagated upstream through the passage. Fourier analysis of the vane surface pressures indicated that the first harmonic pressure fluctuations were as large as 10% of the time average, with significant second and third harmonics also present.

Viscous calculations were also performed with the geometry scaled such that each blade row was represented as a single passage. This had a dramatic effect on the upstream vane-reflected wave pattern. These wave reflections induced unsteady flow separation on both vane surfaces, with separation bubbles evolving and vanishing over a single blade-passing period.

Liamis et al.[4] analyzed transonic rotor–IGV interactions using a quasi-three-dimensional Navier–Stokes analysis and reported similar results. Namely, the rotor shocks generated pressure waves in the IGV passage that interacted with the boundary layers as they reflected off the vanes. This caused the IGV outlet flow angle and velocity to vary significantly over one blade-passing period.

Micklow et al.[5] investigated the effects of geometry scaling on rotor–stator interactions in a transonic compressor stage with a quasi-three-dimensional thin-layer Navier–Stokes analysis. For the first simulation, the actual geometry with 12 rotor and 30 stator airfoils was modeled by 2 rotor and 5 stator passages. In the second simulation, the stator geometry was scaled to maintain solidity and reduce the computational domain to one rotor and two stator passages. These simulations revealed that geometry scaling to reduce CPU time and storage requirements led to greater unsteady interaction effects that resulted in increased loss and lower stage performance.

Laser Doppler velocimetry has been the most common method for investigating flowfields. This is a nonintrusive technique that provides statistical information about the velocity at a given point in the flow. Because it is a point measurement technique, the velocity field is determined by traversing the probe volume over a relatively coarse grid in the region of interest.

Particle image velocimetry (PIV) is a relatively new whole-field technique that provides quantitative measurement and visualization of a two-dimensional velocity field. In this technique, seed particles within the region of interest are illuminated by a thin light sheet generated by a double-pulsed, high-power laser, with images of the

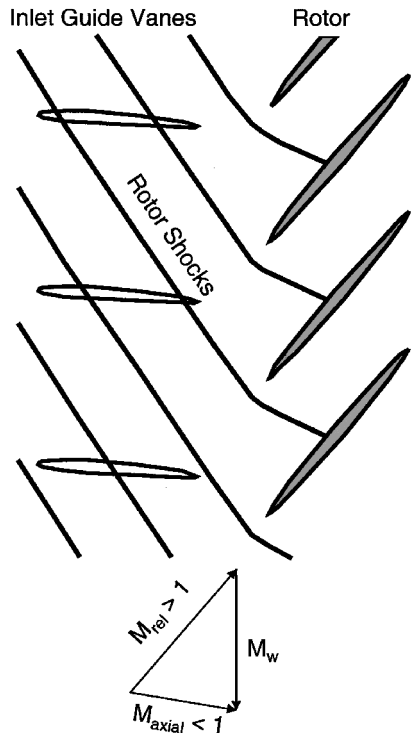

Fig. 1 IGV excitation caused by rotor leading-edge shock waves.

particles corresponding to the first and second laser pulse recorded. The distances traveled by the particles over this time interval are determined using correlation algorithms, with the velocity field calculated by dividing each distance by the known time between pulses. The result is an instantaneous measurement of the velocity field at a single instant in time, which allows quantitative visualization of flowfield structures that would be difficult if not impossible to obtain using point measurement techniques.

PIV applications to turbomachinery include measurements in a two-dimensional turbine cascade,[6] a transonic three-dimensional annular turbine nozzle row,[7] a low-speed compressor rotor,[8] and the first-stage vanes of a low-speed turbine with and without leading-edge showerhead film cooling.[9] Funes-Gallanziet al.[10] have also made PIV measurements in the wake region behind an isolated transonic turbine nozzle and reported reasonable agreement with a steady three-dimensional viscous analysis. Day-Treml and Lawless[11] investigated vane–blade interactions in a low-speed turbine, with PIV data acquired between the first-stage vane and rotor. Near the rotor leading-edge plane, the flow underturning in the vane wake was dominated by overturning caused by the periodic passing of the rotor potential field. Ehrlich and Fleeter[12] used PIV to characterize the unsteady flow over an annular cascade airfoil driven to oscillate in a chordwise bending mode. Estevadeordal et al.[13] and Ottavy et al.[14,15] investigated the blade row interactions in a transonic axial-flow compressor and Wernet et al.[16] applied PIV to investigate surge in a high-speed centrifugal compressor.

Time-accurate multistage computational fluid dynamics (CFD) analyses are being utilized to analyze nonlinear blade row interactions in advanced turbomachine designs. However, these solutions are dependent on the particular turbulence model utilized, with the computational domain also reduced by scaling the geometry such that each airfoil row is represented, at most, by a few passages. This greatly reduces storage requirements, but alters the fundamental periodicity of rotor–stator interactions, that is, the interblade phase angle, which is specified by the blade–vane count ratio. Thus, fundamental blade row interaction data are needed to assess the validity of these CFD analyses. These data must include not only aerodynamic forcing function and the resulting airfoil surface unsteady response, but also steady and unsteady flowfield information.

This paper addresses this need, with detailed benchmark rotor–IGV unsteady aerodynamic blade row interaction data acquired in an advanced design transonic multistage research compressor at both design and part-speed operating conditions. These detailed data include PIV measurements of the instantaneous vane-to-vane flowfield in the IGV passage at 90% span, which complements previously acquired IGV surface pressure data.[1]

Research Facility

The Purdue transonic multistage research compressor features a one-and-one-half-stage axial-flow geometry, which is representative of that used in the front stages of advanced aircraft engine high-pressure compressor designs. The drive system consists of a 400-hp ac motor, a variable-speed magnetic clutch, and an 8:1 ratio gearbox, the output of which drives the compressor rotor (Fig. 2). Atmospheric air is drawn into the test section through a converging bellmouth inlet with a 16:1 contraction ratio and exits the test section through discharge piping, which contains a butterfly throttle valve to regulate the flow rate.

The test section has a constant hub–tip ratio of 0.67 with a tip diameter of 0.3 m (12.0 in.) and features an IGV row, a blisk with 19 rotor blades, and a downstream stator. The compressor design speed is 20,000 rpm, with a maximum pressure ratio of 1.38. The rotor blades consist of NACA 65 series profiles on circular arc meanlines with a 5.08-cm (2.0 in.-) chord and a thickness distribution varying from 10% at the root to 6% at the tip. Because this is a subsonic-design rotor, operation at transonic speeds results in a strong bow shock. The IGV and stator vanes are an advanced controlled diffusion airfoil design with a 4.45-cm (1.75 in.-) chord and a constant 7% thickness. Both the IGV row and the stator feature variable stagger angles and adjustable axial spacings and can be independently configured with either 18 or 20 vanes. Additionally, the IGV row is indexable, that is, the IGV ring can be clocked circumferentially relative to the downstream stator and stationary instrumentation probes.

PIV

PIV is a whole-field measurement technique, providing quantitative flow visualization of a two-dimensional velocity field. The flow is seeded with tracer particles, with the two-dimensional blade-to-blade plane of interest illuminated by a laser sheet generated by a timed double pulse of a high-power laser. In the digital PIV technique, a charge-coupled device (CCD) camera synchronized to the laser is used to record the images of the seed particles within the light sheet for both laser pulses. The camera images are then divided into rectangular interrogation regions, and correlation algorithms are used to determine an average displacement vector for each region. The velocity vectors are then determined by dividing each displacement vector by the specified time between pulses.

The DANTEC PIV system utilized for these experiments consists of a 30-mJ NewWave Research Minilase III Nd:YAG laser, a high-resolution Kodak Megaplus ES 1.0 digital camera, and a dedicated personal-computer-controlled PIV 2100 Processor. The laser has twin oscillators operated in single Q-switch mode and is capable of delivering a 5–7 ns duration pulse with a wavelength of 532 nm (visible green light) at a repetition rate of 10 Hz. The two oscillators are necessary to provide a pair of equal energy laser pulses in the short time interval required to expose the images in a high-speed flow, with the time between pulses specified using software. The digital camera has a 1008×1018 CCD array operated in cross-correlation mode, with the images corresponding to the first and second pulse of the laser recorded separately, with the minimum allowable time between these frames 1 μs. Both images are then transferred to the PIV 2100 Processor that provides near real-time vector processing of the images using fast Fourier transform (FFT) correlation techniques. This unit also synchronizes the camera and laser and is capable of resolving the particle displacement to within $\frac{1}{10}$ of a pixel through the use of subpixel interpolation schemes. Personal-computer-controlled software is used to perform offline validation and postprocessing of the vector maps, with directional

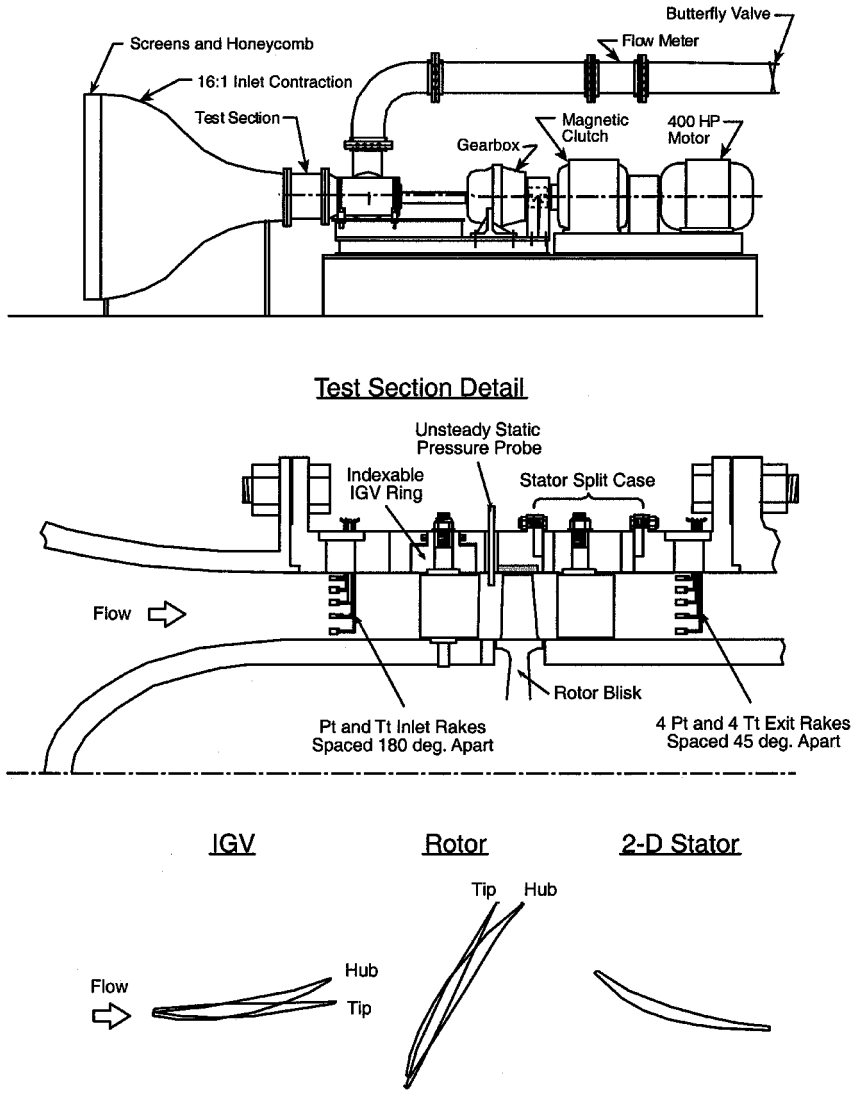

Fig. 2 Purdue transonic multistage axial compressor research facility.

velocity information unambiguously determined because the initial and final particle positions are recorded as separate images.

Reliable PIV measurements require that the flow be seeded with tracer particles small enough to track the flow accurately and large enough to scatter sufficient light to be detected with the imaging system. These particles must be introduced in a manner that does not significantly disturb the flowfield and at the same time provide a sufficient and uniform seeding density in the region of interest. Because of the high flow rate through the compressor, a Rosco 1600 fog machine is used to generate the seed particles. This is a thermal aerosol generator that produces a high volume of seed particles by discharging a heated and pressurized glycol-based mixture into the atmosphere where it immediately vaporizes and then condenses into a fine mist of monodisperse particles. A uniform seeding density in the test section is achieved by introducing these seed particles upstream of the bellmouth inlet and allowing them to disperse into the ambient air before being drawn through the facility.

To characterize the unsteady flowfield generated by the rotor–IGV interactions, the instantaneous IGV vane-to-vane flowfield is measured at 90% span for several time instants over one rotor blade-passing period. A once-per-revolution pulse from a photooptic sensor on the compressor shaft triggers the PIV 2100 Processor that then fires the lasers and records the camera CCD images. To record images at different points over one periodic cycle, the measured rotor speed is used to calculate the time delay to position the rotor at the desired angular location relative to the stationary vanes. This value is then programmed into a LaserStrobe 165 phase delay generator, which can deliver an accurate time delay up to 999.9 μs in 0.1 μs increments.

The IGV vane-to-vane flowfield at 90% span is illuminated by a 1-mm-thick light sheet introduced upstream through the bellmouth inlet section using a combination of cylindrical and spherical lenses. Optical access to the IGV passage is provided with a removable 2.54-cm-(1.0-in.-)constant thickness Plexiglas® window contoured to the flow path o.d. (Fig. 3). A 60-mm Nikon lens with an aperture setting of $f/4.0$ was used to image the flow through an entire IGV passage onto the CCD array, an example of which is shown in Fig. 4. This provided information about the global features of the unsteady flowfield generated by rotor–IGV interactions, but the spatial resolution was inadequate to resolve small-scale flow structures.

To examine the details of the flowfield generated by the impact of the rotor shock with the vane surface, a Nikon 105-mm lens was used to image only a small portion of the IGV trailing-edge flowfield. The magnification factors for both lenses were determined by photographing a test grid with known spacing through the window assembly, with optical distortion caused by the curved window accounted for by using separate scale factors in the horizontal and vertical directions.

The images corresponding to the first and second laser pulses are divided into rectangular interrogation areas, with cross-correlation software used to determine an average particle displacement for each region. To obtain a high signal-to-noise ratio, the interrogation

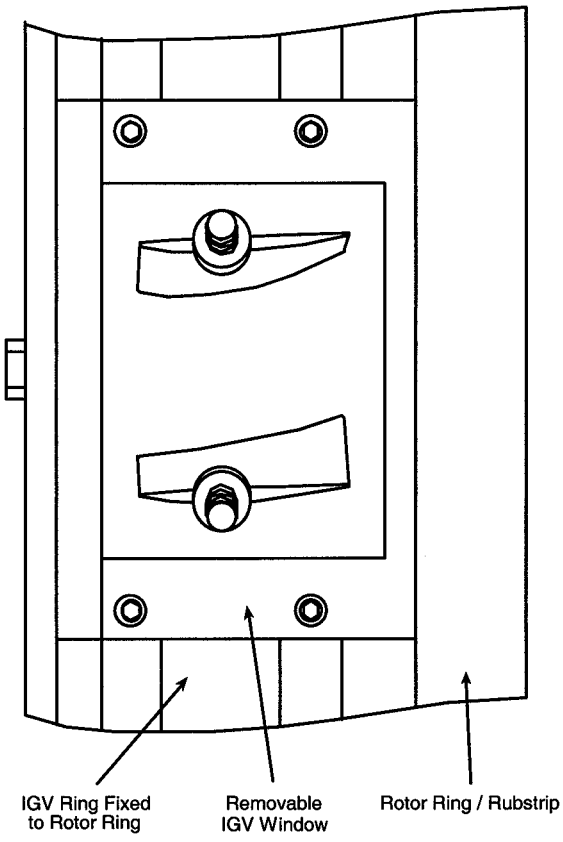

Fig. 3 IGV optical access.

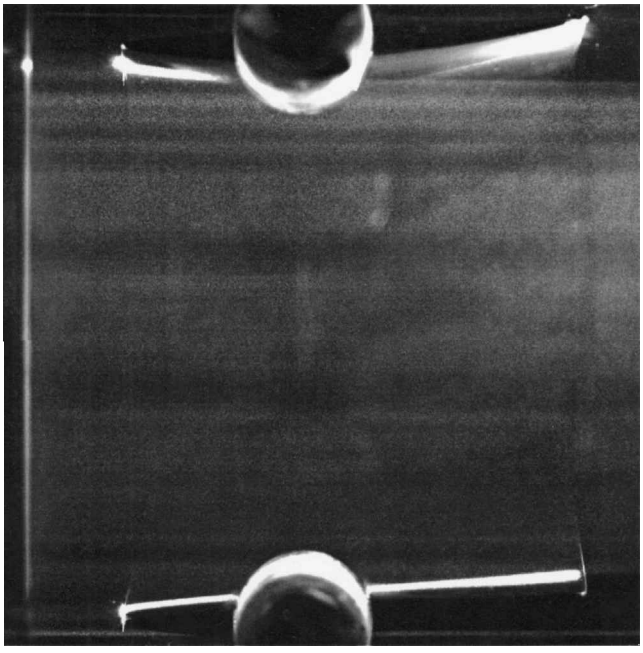

Fig. 4 Raw PIV image.

area must be small enough so that the flow velocity is homogeneous within each region and at the same time large enough to encompass a sufficiently large population of particle pairs. When imaging large areas with high gradients such as unsteady flow through turbomachinery blade passages, it may not be possible to satisfy both of these requirements simultaneously, and a compromise must be made when choosing the size of the interrogation area.

The FFT processing algorithm that computes the cross correlations generates artificial cyclic background noise at the edges of each interrogation area because this approach assumes that the sampled regions are periodic in space. This can result in the loss of particle pairs due to a low signal-to-noise ratio at the boundaries, with particles near the edges not used in the velocity calculation. However, this information is recovered by oversampling the images using overlapping interrogation regions. This process does not increase the fundamental spatial resolution, but generates additional vectors as suitable interpolations. For the present investigation, 32×32 pixel interrogation areas with 50% overlap are used to process the image maps, which results in 3844 raw vectors per image.

Results

The unsteady flowfield in the upstream IGV passage generated by rotor–IGV blade row interaction is investigated at both the transonic design speed and a part-speed condition in which the rotor flow is subsonic. The compressor test section is configured with moderate axial spacings, with the IGV–rotor and rotor–stator midspan axial spacings set at 41.4 and 39.0% vane chord, respectively. Both the IGV and stator have 18 vanes set at their design stagger angles (minimum-loss incidence), with these setting angles identical for both the subsonic and transonic rotor speeds. The IGV row is fixed in the unclocked position, that is, the stacking axes of the IGV and stator vanes coincide at the same circumferential position (Fig. 2).

Compressor and IGV Steady Performance

The compressor performance data define the operating points at which the detailed unsteady aerodynamic data are acquired (Fig. 5). Data are acquired along the nominal operating line (aerodynamic design point) at 75% ($N_c = 15{,}000$ rpm) and 100% ($N_c = 20{,}000$ rpm) design speed.

The time-average IGV surface Mach number distributions are shown in Fig. 6. The distributions are similar for both operating points, with the average IGV inlet Mach number at 0.37 for the transonic design speed and at 0.27 for the part-speed operating condition.

PIV Data Ensemble Averaging

The PIV data are ensemble averaged to obtain clean periodic snapshots of the IGV flowfield at several time instants over one interaction cycle. Figure 7 shows the effect of using different numbers of images to determine the ensemble-averaged Mach number contours for a single frozen rotor blade position at the transonic design speed. The instantaneous flowfield for one ensemble contains a high degree of random unsteadiness, with as few as 15 ensembles sufficient to obtain clean periodic snapshots of the flowfield. Relatively few ensembles are required for the PIV data because the vector fields for each image are constructed using a spatial average of the velocity within each interrogation region, with processing of the image maps averaging out many of the small-scale structures associated with turbulent flow.

Note that there are some regions of the flowfield where it was not possible to acquire valid data. Because the flowfield is turbulent, there is a finite probability that some particles will travel out

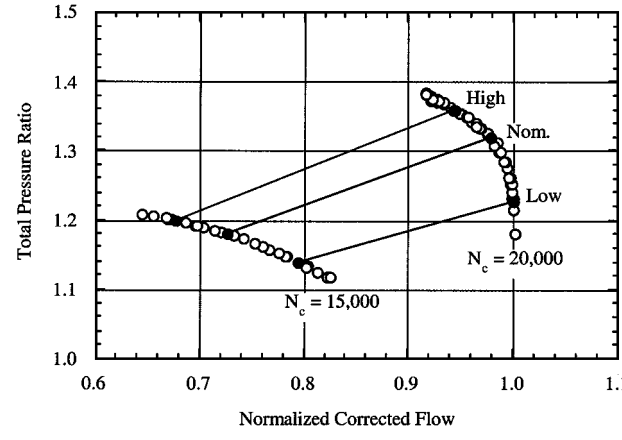

Fig. 5 Compressor performance map.

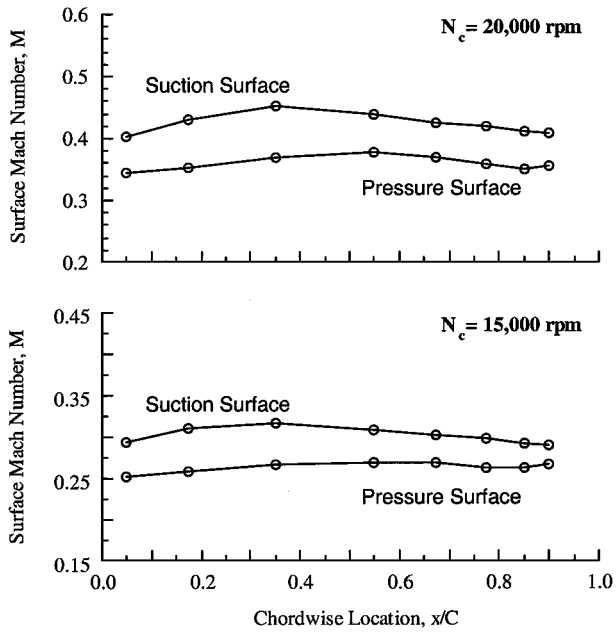

Fig. 6 Time-average IGV surface Mach number for nominal operating line.

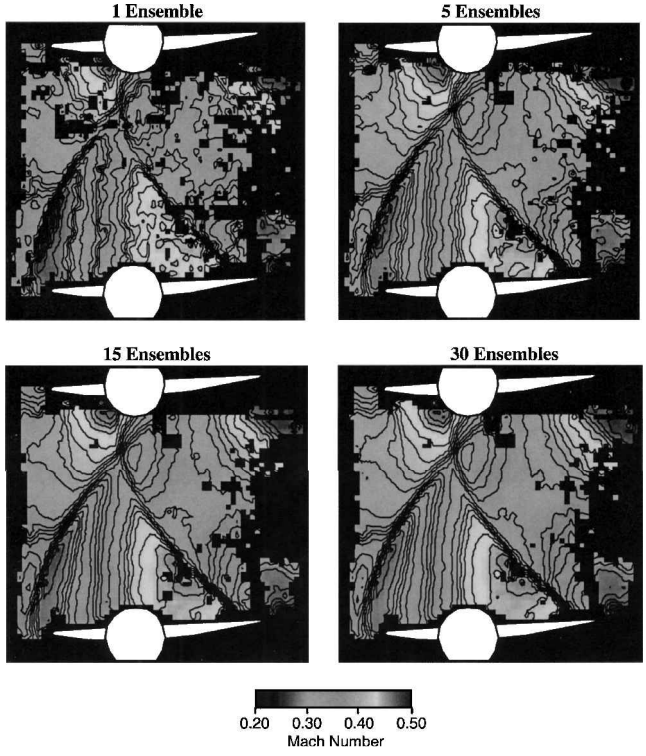

Fig. 7 Effect of ensemble averaging the IGV flowfield at 20,000 rpm.

of the plane of the light sheet between successive images. This loss of particle pairs causes some interrogation regions to yield no valid data, with this loss of data occurring at random locations in each image. Additionally, there are other regions of the flowfield where it was not possible to obtain valid data regardless of the number of ensembles used, that is, near the vane surfaces and passage exit. The lack of data in these regions is attributed to a combination of factors such as saturation of the raw image caused by shadows and reflections off the vane surfaces and secondary reflections off the rotating rotor blades back into the vane passage. Three-dimensional flow effects in the vicinity of the rotor leading edge may also contribute to the lack of data near the passage exit. Thus, in general, the number of valid vectors used to compute the ensemble average flowfield is less than the number of images used, with no valid data present in some regions of the flow. For the subsequent analysis, 30 images are used to calculate the ensemble-averaged velocity field for each rotor position, with at least five valid vectors required to compute the mean for each interrogation area.

Time-Variant IGV Flowfield

The time-variant IGV vane-to-vane flowfield is measured at 90% span using PIV, with ensemble-averaged snapshots of the periodic unsteady flowfield generated by IGV–rotor interactions presented for 10 equally spaced increments over one blade passing period. The time average of the unsteady flowfield is also presented, with this vector field calculated by arithmetically averaging the ensemble-averaged flowfield over one complete cycle. Because it was not possible to obtain data at every point in the flowfield, the time average is calculated only for interrogation regions that had valid velocity vectors at all 10 time instants.

Figures 8 and 9 show the time-average and unsteady Mach number contours over one periodic cycle, respectively, for the transonic rotor speed, with the contours shown in increments of 0.01 and the scales the same for both Figs. 8 and 9. The time-averaged PIV data at the IGV leading-edge plane are in excellent agreement with the average inlet Mach number of 0.37 calculated from the surface pressure data of Fig. 6. The instantaneous snapshots of the flowfield shown in Fig. 9 demonstrate the highly unsteady nature of the flowfield generated by the transonic rotor–IGV interactions and reveal several complicated interaction phenomena. The rotor leading-edge shock waves are reflected and diffracted as they impact the IGV trailing edge (Fig. 10). The reflection point moves upstream as the cycle progresses, with the incident shock decaying as it propagates through the IGV passage. The reflected shock segment, however, travels across the vane passage as it propagates upstream, interacting with the shock of the adjacent rotor blade before it eventually impacts the suction surface of the upper vane in the leading-edge region.

The reflection of the shock by the vane pressure surface causes a significant increase in the static pressure (overpressure zone) in the region aft of the reflection point ($p_3 > p_2$). Because the IGV flow is subsonic, a pressure wave is generated in the trailing-edge region that equalizes the pressure in the overpressure zone with the lower pressure region aft of the diffracted shock on the suction surface. This process is periodic because the shock waves translate with the rotor, with the reflection point moving upstream along the IGV chord and the reflected shock segment continuing to propagate upstream toward the suction surface of the adjacent vane as the cycle

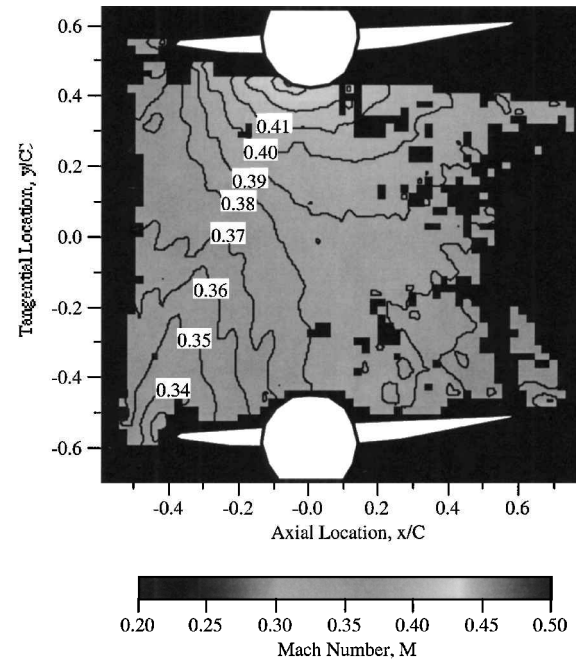

Fig. 8 Time-average IGV flowfield at 20,000 rpm.

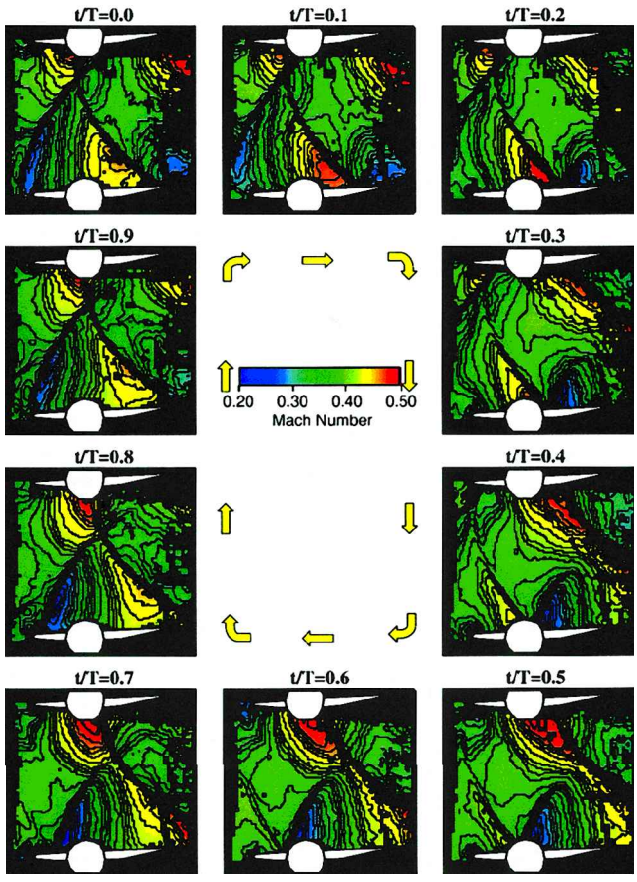

Fig. 9 Time-variant IGV flowfield at 20,000 rpm.

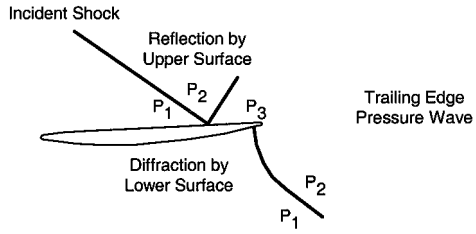

Shock interaction with vane trailing edge

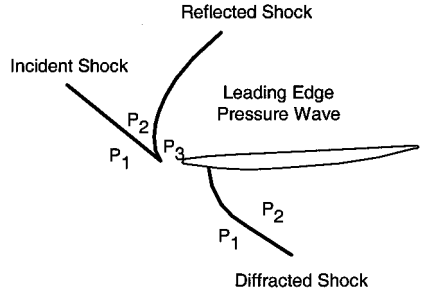

Shock interaction with vane leading edge

Fig. 10 Shock wave interaction with an isolated vane.

progresses. As the reflection point moves past the vane leading edge, another pressure wave is generated near the leading edge to equalize the pressure on the upper and lower surfaces, and the reflected shock segment is diffracted as it bends around the leading edge. Note that cascade effects can cause secondary reflections, with the reflected shock segments impacting adjacent vanes or the multiple leading-edge shocks generated by the rotor as they propagate upstream.

At time $t/T = 0.9$, the rotor leading-edge shock wave is just about to impact the lower vane in the passage. Note, however, that the shock of the adjacent rotor blade has already impacted the upper vane in the passage due to the unequal blade–vane count. The blade–vane count ratio sets the spatial periodicity of unsteady flow phenomena in the passage, with interactions that occur on the upper vane leading those on the lower vane by the interblade phase angle. For the present geometry with 18 IGVs and 19 rotor blades, the interblade phase angle is 380 deg. Thus, it takes any given rotor blade 1.06 blade-passing periods to traverse the IGV passage, with the rotor–IGV interactions for each vane periodic at blade-pass frequency.

At time $t/T = 0.0$, the rotor shock impacts the lower vane and is diffracted as it bends around the trailing edge. At the next time instant, the point of impact has moved upstream, and the shock is reflected by the vane pressure surface. A pressure wave is also generated at the trailing edge to equalize the overpressure region aft of the reflected shock with the lower pressure region on the suction surface behind the diffracted shock. The reflected shock segment continues to propagate upstream toward the suction surface of the upper vane in the passage as the cycle progresses, with the incident shock decaying as the reflection point moves farther upstream along the vane chord and is no longer visible at time $t/T = 0.7$.

At time $t/T = 0.4$, a pressure wave is also visible just ahead of the diffracted shock on the upper vane suction surface. This pressure wave continues to grow and begins interacting with the shock segment reflected by the lower vane at $t/T = 0.6$. This interaction between the pressure wave and the reflected shock segment continues as the cycle progresses, with the reflected shock also beginning to interact with the incident shock generated by the adjacent rotor blade at $t/T = 0.8$. This complex interaction continues as the cycle repeats up until time $t/T = 0.3$, at which point the shock segment reflected by the lower vane during the previous cycle has traveled across the passage and impacts the suction surface of the upper vane in the leading-edge region.

A low-velocity, high-pressure region characterizes the IGV flowfield aft of the reflected shock on the vane pressure surface. After passing through the reflected shock segment, fluid particles are smoothly accelerated to a velocity higher than the freestream before being again decelerated as they pass through the incident shock generated by the adjacent rotor blade. Note that a similar process also occurs on the suction surface of the upper vane in the passage aft of the secondary reflection point.

Figures 11 and 12 show the time-average and unsteady Mach number contours at the same 10 time instants for the part-speed subsonic rotor operating condition, with the contours again shown in increments of 0.01 with the same scales for both Figs. 11 and 12. The time-average subsonic and transonic rotor-generated IGV flowfields are similar, with the time-averaged PIV data at the IGV leading-edge plane again in excellent agreement with the average inlet Mach number of 0.27 calculated from the surface pressure data. The time-variant snapshots of the flow shown in Fig. 12 closely resemble the time-average flow throughout the entire cycle. This is due to the subsonic rotor potential field imposing a mild unsteady backpressure variation on the upstream IGV row, with the flow through the IGV passage smoothly responding to the passing of the rotor at each time instant. This is in contrast to the highly unsteady flowfield generated at the transonic rotor speed in which the rotor leading-edge shocks were reflected and diffracted as they interacted with the upstream vane row, creating sharp unsteady velocity gradients in the IGV flow.

Time-Variant Trailing-Edge Flowfield

To examine the detailed unsteady flowfield generated by the impact of the rotor shocks with the vane trailing edge, PIV images were also acquired focusing on a small portion of the trailing-edge flowfield. Figure 13 shows the time-average streamlines in the trailing-edge region of the lower vane superimposed on the Mach number contours for the transonic rotor speed. The streamline patterns indicate that the time-average flowfield is two dimensional, uniform, and tangent to the vane surface throughout the entire trailing-edge region. It was not possible to obtain images of the vane suction surface in this region due to the airfoil curvature creating a shadow in the region aft of the stacking axis at 39% chord.

The trailing-edge Mach number contours for the same 10 time instants used to examine the vane-to-vane flowfield are shown with

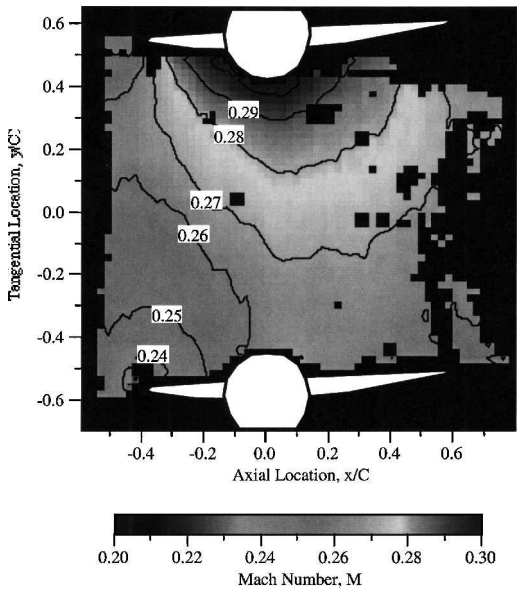

Fig. 11 Time-average IGV flowfield at 15,000 rpm.

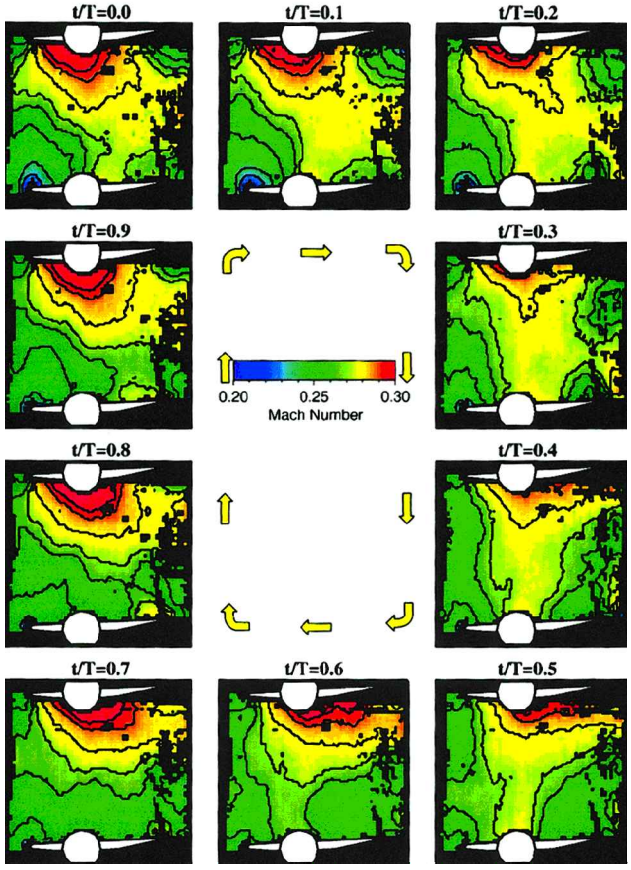

Fig. 12 Time-variant IGV flowfield at 15,000 rpm.

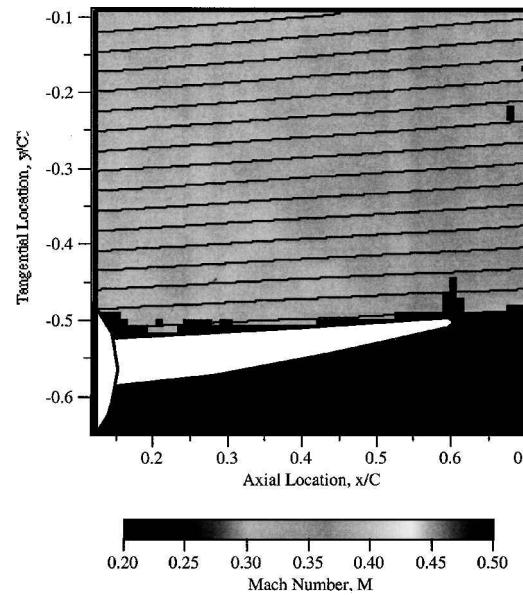

Fig. 13 Time-average IGV streamlines in trailing-edge region at 20,000 rpm.

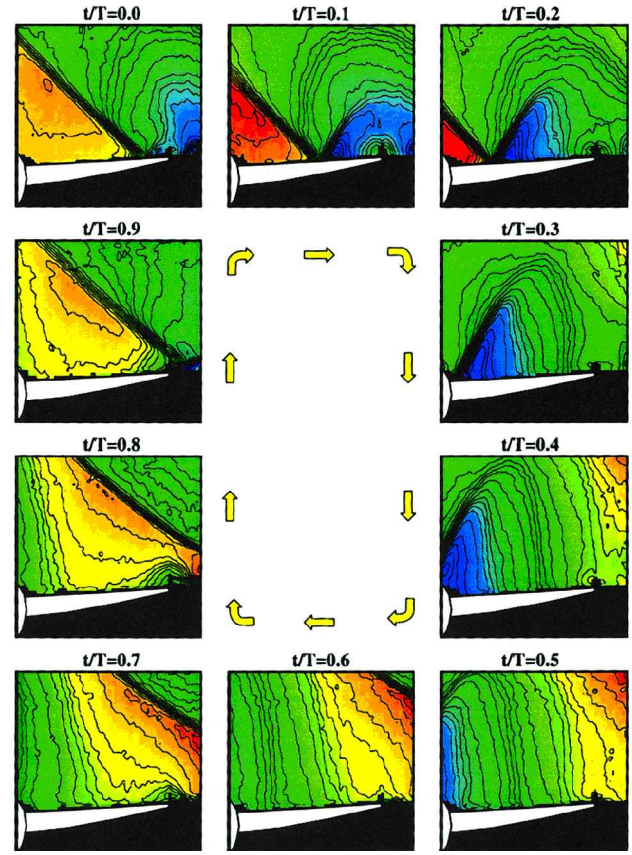

Fig. 14 Time-variant IGV flowfield in trailing-edge region at 20,000 rpm.

the same scales and contour increments in Fig. 14. The time-variant images clearly show the sharp flowfield gradients caused by the rotor leading-edge shocks and the detailed interaction process that occurs when they impact the vane surface. Note the low-velocity region present near the vane trailing edge before the impact of the rotor shock. This region is attributed to the periodic movement of the trailing-edge stagnation point from the upper to the lower surface caused by the large unsteady backpressure variation generated by the rotor shocks. This phenomenon was not evident in the vane-to-vane flowfield images due to insufficient spatial resolution to resolve these small-scale flow structures.

At time $t/T = 0.0$, the rotor leading-edge shock impacts the vane and is in the process of being diffracted by the IGV trailing edge, with a pressure surface reflection not yet evident. At the next time instant, the incident shock has been diffracted by the trailing edge, and a regular-type reflection occurs on the pressure surface, that is, the reflection occurs at the solid boundary and the incident and reflected waves make approximately the same angle with the vane. The reflection process generates a significant pressure rise in the region aft of the reflected shock segment, with this pressure greater

than the corresponding pressure aft of the diffracted shock on the lower vane surface (Fig. 10). This overpressure region causes the flow to accelerate around the vane trailing edge toward the lower pressure region on the suction surface, with the stagnation point or dividing streamline occurring on the lower surface. This acceleration region is shown by the semicircular Mach number contours emanating from the trailing edge at time $t/T = 0.1$.

Because the IGV flowfield is subsonic, a pressure wave is generated at the trailing edge to equalize the pressure on the upper and lower vane surfaces. As this wave is generated, the stagnation point moves along the IGV suction surface toward the trailing edge, and the pressure surface acceleration region is diminished, with its effect no longer visible by time $t/T = 0.3$. As the cycle progresses, the unsteady backpressure associated with the passing of the rotor causes the stagnation point to move around the trailing edge and up onto the vane pressure surface. This effect is first visible at time $t/T = 0.7$, with a low-velocity region forming near the trailing edge as the flow decelerates ahead of the stagnation point. This low-velocity region increases in size as the stagnation point moves farther upstream until time $t/T = 0.8$, after which its effects start to diminish and are no longer visible by time $t/T = 0.0$, at which point the cycle repeats.

This process is further illustrated in Fig. 15, which shows the unsteady velocity vectors superimposed on the time-variant Mach number contours. This unsteady velocity field was calculated by subtracting off the time-average velocity and shows how the steady flowfield is perturbed at each time instant. Note that reversed flow regions are not evident as the stagnation point periodically moves from the upper to the lower surface of the vane. This is because the unsteady upwash velocity associated with the rotor passing, that is, the unsteady aerodynamic forcing function to the IGVs, is superimposed on the velocity field of the responding vane row, and effects of each cannot be distinguished from one another. The vectors do, however, indicate increased perturbations in the vicinity of the IGV trailing edge as the stagnation point moves from the upper to the lower surface.

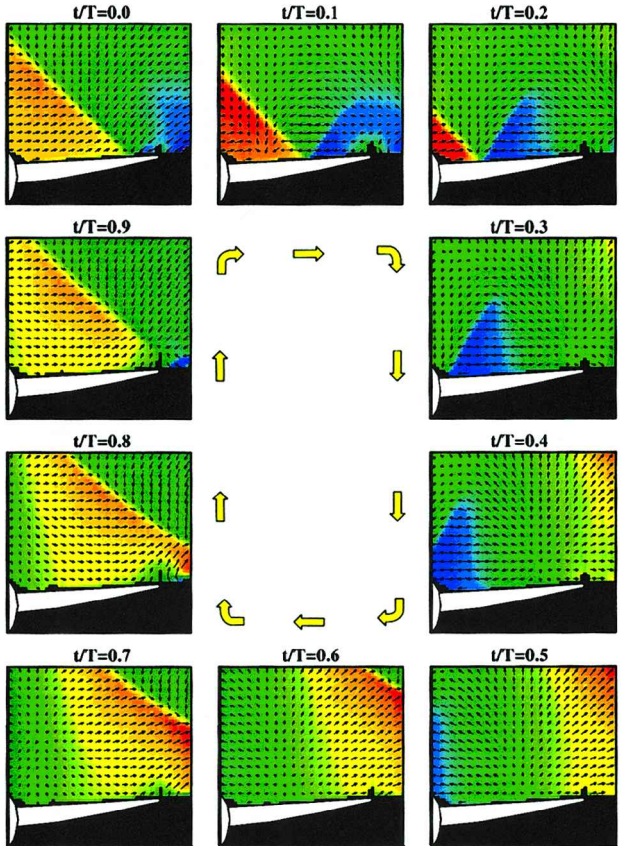

Fig. 15 IGV unsteady vector field in trailing-edge region at 20,000 rpm.

Summary

The rotor–IGV interactions in an advanced design multistage axial compressor at both transonic and subsonic rotor operating conditions were investigated using PIV. The resulting vane-to-vane flowfield data complement previous IGV surface pressure and forcing function measurements and provide a benchmark test case for CFD code validation.

For the part-speed rotor operating condition, the time-variant IGV flowfield closely resembled the time-average flow throughout the entire cycle. This was due to the subsonic rotor potential field imposing a mild unsteady backpressure variation on the upstream vane row, with the flow through the IGV passage smoothly responding to the passing of the rotor at each time instant.

The time-variant IGV flowfield at the transonic design speed differed markedly from the time-average vane-to-vane flow. The impact of the rotor leading-edge shocks with the vane trailing edge resulted in the incident shock being reflected by the pressure surface and diffracted by the suction surface. The reflection point moved upstream as the cycle progressed, with the incident shock decaying due to its interaction with the vane row as it propagated upstream through the vane passage. The reflected shock segment, however, did not decay and traveled across the vane passage as it propagated upstream, interacting with the incident shock of the adjacent rotor blade before it eventually impacted the suction surface of the upper vane in the leading-edge region. This interaction resulted in a complicated time-dependent wave pattern being established in the vane passage, with steep velocity gradients occurring across both the incident and reflected shocks.

The reflection of the rotor shock by the upstream vanes generated a high-overpressure zone aft of the reflection point on the vane pressure surface. This high-pressure region caused the flow to accelerate around the trailing edge and the stagnation point to move periodically from the upper to the lower surface of the vane over the course of a single blade-passing period. This effect was not evident, however, in previous unsteady surface pressure measurements because the placement of the last transducer was at 90% chord due to the finite trailing-edge thickness.

Acknowledgments

This research was sponsored by the Air Force Office of Scientific Research and Pratt and Whitney Aircraft, United Technologies Corporation. This support is most gratefully acknowledged.

References

[1]Sanders, A. J., and Fleeter, S., "An Experimental Investigation of IGV-Rotor Interactions in a Transonic Axial-Flow Compressor," *Journal of Propulsion and Power*, Vol. 38, No. 2, 2000, pp. 284–291.

[2]Silkowski, P. D., Copeland, G. S., Eley, J. A., Bleeg, J. M., and Rhie, C. M., "CFD Investigations of Aeromechanics," American Society of Mechanical Engineers, ASME Paper 2001-GT-0267, June 2001.

[3]Eulitz, F., Engel, K., and Pokorny, S., "Numerical Investigation of Inviscid and Viscous Interaction in a Transonic Compressor," *Propulsion and Energetics Panel 85th Symposium*, CP-571, Paper 38, AGARD, 1995.

[4]Liamis, N., Bacha, J. L., and Burgaud, F., "Numerical Simulations of Stator-Rotor Interactions on Compressor Blade Rows," *Propulsion and Energetics Panel 85th Symposium*, CP-571, Paper 36, AGARD, 1995.

[5]Micklow, G. J., Sauve, J. P., and Shivaraman, K., "Numerical Simulations of Advanced Transonic Compressor Stages Using an Unsteady Quasi-Three-Dimensional Flow Solver," American Society of Mechanical Engineers, ASME Paper 95-GT-440, 1995.

[6]Post, M. E., Goss, L. P., and Brainard, L. F., "Two-Color Particle-Imaging Velocimetry in a Turbine Cascade," AIAA Paper 91-0274, 1991.

[7]Bryanston-Cross, P. J., Towers, C. E., Judge, T. R., Towers, D. P., Harasgama, S. P., and Hopwood, S. T., "The Application of Particle Image Velocimetry (PIV) in a Short-Duration Transonic Annular Turbine Cascade," *Journal of Turbomachinery*, Vol. 114, July 1992, pp. 504–509.

[8]Tisserant, D., and Breugelmans, F. A. E., "Rotor Blade-to-Blade Measurements Using Particle Image Velocimetry," American Society of Mechanical Engineers, ASME Paper 95-GT-99, 1995.

[9]Day, K. M., Lawless, P. B., and Fleeter, S., "Particle Image Velocimetry Measurements in a Low-Speed Research Turbine," AIAA Paper 96-2569, 1996.

[10]Funes-Gallanzi, M., Bryanston-Cross, P. J., and Chana, K. S., "Wake Region Measurements of a Highly Three-Dimensional Nozzle Guide Vane Tested at DRA Pyestock using Particle Image Velocimetry," American Society of Mechanical Engineers, ASME Paper 94-GT-349, 1994.

[11]Day-Treml, K. M., and Lawless, P. B., "Particle Image Velocimetry of Vane–Rotor Interaction in a Turbine Stage," AIAA Paper 98-3599, 1998.

[12]Ehrlich, D. A., and Fleeter, S., "Particle Image Velocimetry Characterization of a Chordwise Bending Cascade Flowfield," AIAA Paper 97-3022, 1997.

[13]Estevadeordal, J., Gogineni, S., Goss, L., Copenhaver, W., and Gorrell, S., "Study of Flowfield Interactions in a Transonic Compressor Using DPIV," AIAA Paper 2000-0378, Jan. 2000.

[14]Ottavy, X., Trebinjac, I., and Vouillarmet, A., "Analysis of the Inter-Row Flow Field Within a Transonic Axial Compressor: Part 1 Experimental Investigation," *Journal of Turbomachinery*, Vol. 123, No. 1, 2001, pp. 49–56.

[15]Ottavy, X., Trebinjac, I., and Vouillarmet, A., "Analysis of the Inter-Row Flow Field Within a Transonic Axial Compressor: Part 2 Unsteady Flow Analysis," *Journal of Turbomachinery*, Vol. 123, No. 1, 2001, pp. 57–63.

[16]Wernet, W. P., Bright, M. M., and Skoch, G. J., "An Investigation of Surge in a High-Seed Centrifugal Compressor Using Digital PIV," *Journal of Turbomachinery*, Vol. 123, No. 2, 2001, pp. 418–428.